Self-Assembling of Novel Fullerene-Grafted Donor–Acceptor Rod−Coil Block Copolymers

Sophie Barrau and Thomas Heiser*

Institut d'Electronique du Solide et des Systèmes,CNRS UMR 7163, 23 rue du Loess, 67037 Strasbourg, France

Fanny Richard, Cyril Brochon,* Chheng Ngov, Karin van de Wetering, and Georges Hadziioannou

Laboratoire d'Ingénierie des Polymères pour les Hautes Technologies, CNRS UMR 7165, Université Louis Pasteur, Ecole Européenne de Chimie, Polymères et Matériaux, 25 rue Becquerel, 67087 Strasbourg, France

Denis V. Anokhin and Dimitri A. Ivanov*

Institut de Chimie des Surfaces et Interfaces, CNRS UPR 9069, 15 rue Jean Starcky, 68057 Mulhouse, France

Received October 3, 2007; Revised Manuscript Received January 17, 2008

ABSTRACT: Fullerene-grafted rod−coil block copolymers, designed for being used as active polymer layers in donor–acceptor bulk heterojunction photovoltaic devices, have been synthesized. The copolymer synthesis was monitored by ^{1}H nuclear magnetic resonance, size exclusion chromatography and infrared absorption spectroscopy, while the material properties were explored by X-ray diffraction, atomic force microscopy, UV–vis absorption, and photoluminescence spectroscopy. Structural properties of bulk materials and thin films were investigated to study the influence of the coil block molecular weight as well as that of the grafted fullerenes on the molecular self-assembling process. The results show that the rod homopolymer is in the crystalline state at ambient temperature and undergoes a phase transition into a smectic-type liquid-crystalline phase at 55 °C. The rod−coil microphase separation enhances interlamellar ordering but destabilizes the intralamellar order, leading to the appearance of a liquid-crystalline phase for the non-fullerene-grafted copolymer at ambient temperature. Adding the fullerene moieties considerably affects the polymer assembling through the growth of fullerene nanocrystals. The latter hinder the formation of the lamellar phase by pinning the coil segments. The identification of the major driving forces that control the molecular self-assembling process allows us to suggest different alternative strategies that can be used as guidelines for the design of new photovoltaic polymer self-assembling materials.

Introduction

Semiconducting conjugated polymers are promising materials for the development of low-cost optoelectronic applications.[1] A lot of efforts have in particular been devoted in recent years to the design of polymer materials for solution-processed photovoltaic devices.[2–10] Relatively high-energy conversion efficiencies (above 5%) were achieved by using blends of poly(phenylenevinylene)s or poly(alkylthiophene)s with fullerene derivatives as photoactive layer. In these systems, the electron-donating polymers and electron-accepting fullerenes form an interpenetrated network, or donor–acceptor bulk heterojunction, with nanometer-sized domains. The resulting large donor–acceptor interface assists exciton dissociation into free charge carriers while the continuous but separate pathways through both domains allow the photogenerated electrons and holes to reach the electrodes.[11] The long-term stability of such devices is, however, inherently restricted by the macrophase separation of the blend constituents. Improving the control over the active layer morphology on the nanometer scale is therefore among the present key issues that need to be addressed to further improve the photovoltaic performances.[12] A possible way toward this goal is to use donor–acceptor functionalized diblock copolymers as active layer instead of donor–acceptor blends.[13–21] It is indeed known that diblock copolymers microphase separate into well-ordered nanostructures with lamella-, cylinder-, or gyroid-like morphologies or into hexagonally close-packed spheres.[22] By using a semiconducting electron-donor polymer block and a second electron-accepting block, it is possible to combine the self-assembling ability of diblock copolymers with the functionality of conjugated molecules. This gives the challenging opportunity to form thermodynamically stable, nanostructured donor–acceptor films whose morphology can be optimized for photovoltaic applications.

Rod−coil donor–acceptor diblock copolymers based on a poly[(2,5-(1,4-dioctyloxy)phenylenevinylene] (DO-PPV) rodlike block and a polystyrene coil block grafted with fullerene moieties have been previously synthesized and used as active layer in photovoltaic devices by one of the author's group.[13] Similar approaches using diblock copolymers bearing electron-donating and electron-accepting moieties have been reported by Lindner et al.[16,19] and Sun et al.[15] Although the experimental results confirm in all cases a gain in efficiency when using diblock copolymers as active layer instead of the corresponding homopolymer blends, the overall efficiency remained low. These initial studies put a significant effort into the challenging syntheses of complex donor–acceptor molecules. Yet, a more profound comprehension of the resulting nanostructures is needed before the remarkable properties of these polymers can contribute to improve photovoltaic device performances.

* Corresponding authors: E-mail: Thomas.Heiser@iness.c-strasbourg.fr; brochonc@ecpm.u-strasbg.fr; Dimtri.Ivanov@uha.fr.

10.1021/ma7022099 CCC: $40.75
Published on Web 03/13/2008

The self-assembling mechanism and physical properties of diblock copolymers including conjugated segments are far less understood than those of more common coil−coil copolymers. While Gaussian models apply to coil−coil systems for which microphase separation dominates molecular self-assembling, conjugated rod blocks bring in rigid hard-core constraints modulating the local molecular arrangement.[23] Anisotropic interactions of rods give rise to liquid-crystalline and crystalline phases which influence the material thermodynamics and lead to equilibrium structures differing significantly from those of coil−coil systems. Therefore, theoretical models which have been developed successfully to describe coil−coil block copolymer phase separation generally do not apply to the complex "photovoltaic" diblock copolymers. Recently, Olsen et al. investigated the structure and thermal properties of weakly and moderately segregated rod−coil polymers consisting of poly[(2,5-di(2′-ethyl)hexyloxy)-1,4-phenylenevinylene] (DEH-PPV) rod blocks and polyisoprene coil blocks.[24–26] However, since the coil block did not possess an electronic function, the corresponding copolymer cannot be used as such in photovoltaic devices.

In the present work, we investigate rod−coil systems based on DEH-PPV rod blocks with functionalized poly(butyl acrylate-*stat*-chloromethylstyrene) coil blocks. The higher solubility of the DEH-PPV block, with respect to DO-PPV, allows access to good thin film properties. Also, the lower glass transition temperature of poly(butyl acrylate-*stat*-chloromethylstyrene), in comparison to the previously investigated polystyrene coil block, leads to a higher molecular mobility, while its chemical structure enhances segregation. Together, both factors are expected to assist microphase separation both kinetically and thermodynamically.[27] The chloromethylstyrene units allow the grafting of C_{60} molecules onto the coil block and the achievement of donor–acceptor diblock copolymers. The major goal of this work is to study the influence of the coil block fullerene functionalization on the self-assembling process and to outline experimental conditions which may lead to an appropriate thin film nanostructure for photovoltaic applications. We therefore performed a comparative study of the structure and phase behavior of respectively rodlike homopolymers, rod−coil diblock copolymers without grafted C_{60} molecules, and rod−coil diblock copolymers with a fixed amount of fullerene moieties. Both bulk and thin film properties have been investigated.

Experimental Results

Copolymers Synthesis and Functionalization. The rod−coil copolymers were synthesized using poly[(2,5-di(2′-ethyl)hexyloxy)-1,4-phenylenevinylene] (DEH-PPV) end-capped with 2,2,5-trimethyl-4-phenyl-3-azahexane-3-oxyl nitroxide (TIPNO) as initiator for the nitroxide-mediated radical polymerization (NMRP) of the coil block (see Scheme 1). The molecular properties of representative polymers obtained by using different butylacrylate (BA)/chloromethylstyrene (CMS) ratios, polymer/monomer feed ratios, and polymerization times are summarized in Table 1. The copolymers are labeled from **2a** to **2g** following an increasing coil weight fraction. The homopolymer **1** molecular weight ($M_{n,rod}$) of 3.3 kg/mol corresponds to 9.25 monomer units and a total block length of ∼6.5 nm (estimated by assuming a planar homopolymer conformation). We used this polymer as macroinitiator for most copolymers, except for **2b** and **2e**, for which a homopolymer with a molecular weight of 4 kg mol^{-1} and a polydispersity index of 1.3 was used.[27] The coil-block degree of polymerization (DP_n) was estimated from the ^{1}H NMR spectra. By comparing the OCH_2 proton peaks of the DEH-PPV side chains ((4n + 4)H) at δ = 4.0 ppm or, in case of peak overlap, the aromatic peaks of the DEH-PPV, to BA CH_2 aliphatic chain peaks and CMS CH_2Cl peaks, an

Scheme 1. Synthesis of Butyl Acrylate-Based Rod−Coil Copolymers 2 and 3 by NMRP from DEH-PPV-TIPNO Macroinitiator (1)

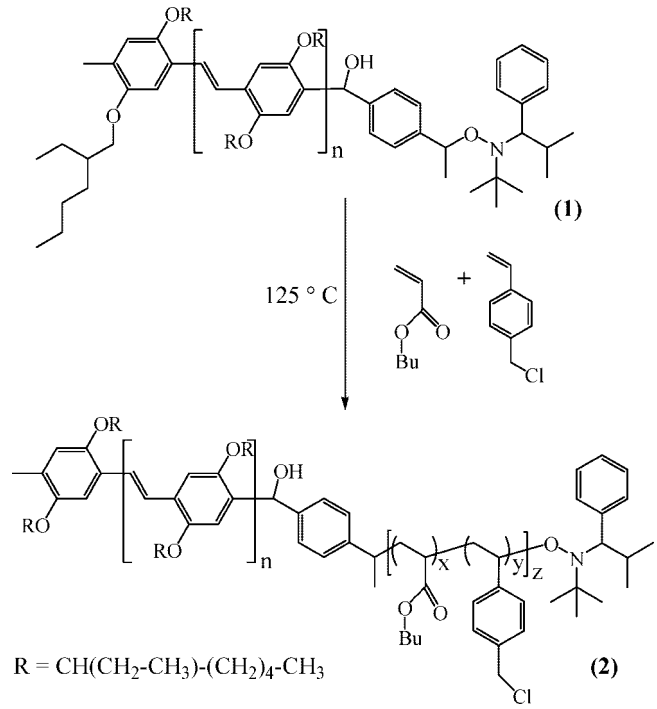

R = $CH(CH_2\text{-}CH_3)\text{-}(CH_2)_4\text{-}CH_3$

Bu = $CH_2\text{-}CH_2\text{-}CH_2\text{-}CH_3$

estimation of the number of BA and CMS monomers incorporated into the copolymer could be performed. The resulting copolymer composition shows that the BA/CMS built-in ratio is lower than the feed ratio. This is due to a higher reactivity of the CMS monomer, implying a preference in adding CMS instead of BA into the copolymers. The copolymer composition can be controlled by adjusting the feed ratio. Different polymerization times were tried. For a short duration of 7 min, no coil block could be detected, indicating an inhibition time which can be attributed to the presence of impurity-related radical traps in the conjugating macroinitiator. During this period, formed radicals are destroyed by consuming the impurities. Its effect on the reaction kinetics is therefore more visible for short reaction times. For a given polymerization time, the starting solution composition determines the reaction kinetics. For instance, using two different BA/CMS ratios, coil block molecular weights ($M_{n,coil}$) of 6.2 (**2c**) and 23.1 kg mol^{-1} (**2f**) (corresponding to a conversion of 5% and 30%, respectively) have been obtained after 40 min of polymerization. At even longer polymerization times, the high conversion leads to very high degrees of polymerization (**2g**). The linear increase of $M_{n,coil}$ with conversion confirms the "living" character of the NMRP copolymerization. It leads from low to moderate polydispersities of the P(BA-*stat*-CMS) block.

The block copolymer with an average of 2.55 CMS units per molecule and with a coil−block weight ratio close to 50% (**2d** in Table 1) was used for the subsequent C_{60} grafting reaction (Scheme 2). Note that copolymers with larger amounts of C_{60} (up to 30 fullerenes per molecule) have also been synthesized but were not further investigated.

The FTIR spectra obtained on homopolymer **1**, on copolymer **2d**, before and after fullerene grafting, and on the intermediate compound DEH-PPV-*b*-P(BA-*stat*-N_3MS) revealed several absorption bands which are due to the coil block (the spectra can be seen in the Supporting Information). An absorption band at 2097 cm^{-1}, which is only observed in the intermediate compound and in the fullerene grafted copolymer with signifi-

Table 1. Molecular Properties of Synthesized Products Characterized by (a) ^{1}H NMR and (b) GPC

		DEH-PPV-*b*-P(BA-*stat*-CMS) (**2**)						
sample label	DEH-PPV **1**	**2a**[f,g]	**2b**[e,h]	**2c**[e,g]	**2d**[f,g]	**2e**[e,h]	**2f**[f,g]	**2g**[f,g]
monomer/polymer molar feed ratio		512	515	517	512	515	513	515
BA/CMS molar feed ratio		22.3	33.3	27.69	22.3	33.3	9.5	29.2
BA/CMS polymer composition		none	12.0	7.10	8.90	10.5	1.44	8.4
polymerization time (min)		7	40	40	195	80	40	195
conversion P[a,b]			0.038	0.033	0.049	0.089	0.292	0.534
coil block degree of polymerization, DP_n[a]		0	21.5	16.6	25.2	46.1	142.1	272.0
M_n[a] (kg mol^{-1})	3.3	3.3	6.8	6.2	6.9	10	23.1	39.0
M_n[c] (kg mol^{-1})	3.2		6.2	6.9	4.8	9.8	23.6	26.6
PDI[c]	1.5		1.6	1.3	1.5	1.6	1.8	1.3
coil (wt %)[d]			36	41	47	56	84	90
observations	WAXS SAXS AFM		AFM	WAXS AFM	WAXS/SAXS	AFM	WAXS AFM	WAXS

[a] Determined by ^{1}H NMR. [b] $P = M_{n,coil}/M_{n,coil,max}$; $M_{n,coil} = M_n^a - M_{n,rod+TIPNO}$. [c] Determined by GPC measurement; RI signal with polystyrene standard. [d] Defined as $M_{n,coil}/(M_n^a - M_{n,rod+TIPNO})$. [e] Sealed tube. [f] Pressure tube. [g] $M_{n,rod} = 3.3$ kg mol^{-1}. [h] $M_{n,rod} = 4$ kg mol^{-1}.

Scheme 2. Grafting of C_{60} on Butyl Acrylate/PPV-Based Rod−Coil Copolymer: (i) NaN_3 in DMF for 24 h at 50 °C; (ii) C_{60} in Dichlorobenzene at 60 °C for 24 h and 120 °C for 1 h

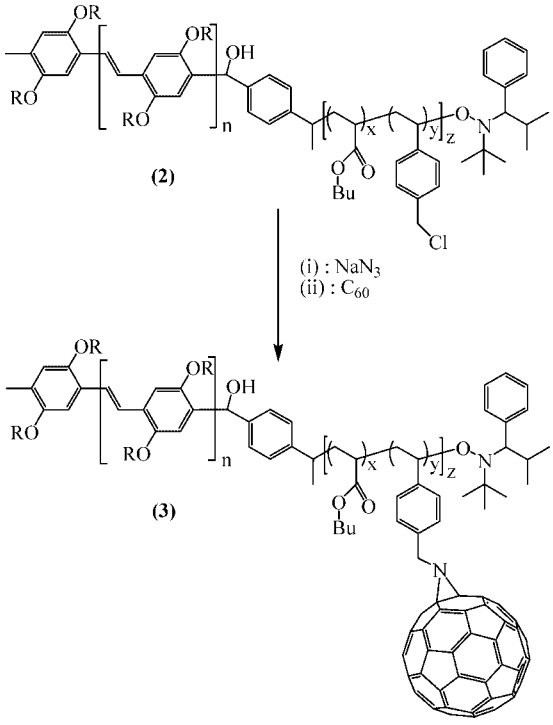

cantly lower intensity, can be attributed to the C−N_3 bond stretching. Its intensity is strongly reduced in the fullerene grafted copolymer **3** due to the replacement of N_3 by C_{60}. The residual amplitude indicates that the conversion reaction may not be complete. Accordingly, the unreacted C_{60} present in our material after synthesis corresponds to at most 10% of the total fullerene content. To reduce the amount of free C_{60}, the reaction product was additionally purified by evaporation of the DCB under reduced pressure, solubilization in chloroform, and filtration to eliminate free C_{60} aggregates.

A comparative ^{1}H NMR analysis of compound **3** and of the intermediate compound, DEH-PPV-*b*-P(BA-*stat*-N_3MS), before purification, showed that the peak corresponding to the protons of the CH_2−N_3 (4.3 ppm) dissappears after fullerene grafting. The residual azide groups seen by FTIR are however below the detection limit of our NMR equipment.

Structural Properties. *Homopolymer.* The wide-angle X-ray diffraction pattern of the homopolymer **1** at ambient temperature is shown in Figure 1. A large number of diffraction peaks are

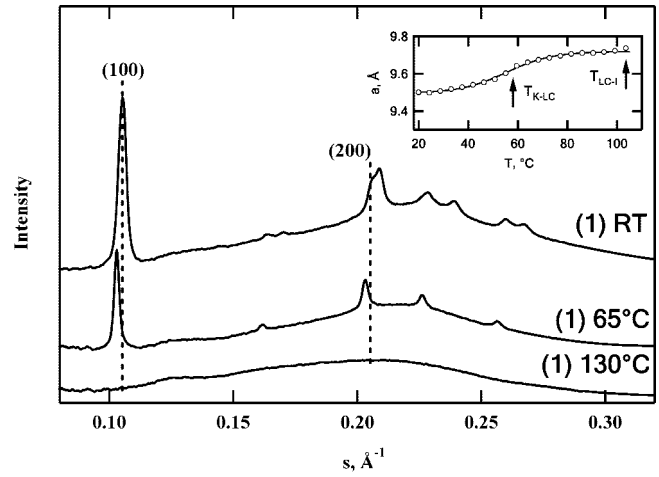

Figure 1. WAXS diffractograms of DEH-PPV (1) measured at room temperature, at 65 °C, and at 130 °C. The inset shows the variation of the *a* parameter of the DEH-PPV unit cell with temperature. The line is a guide for the eye.

Table 2. Experimental and Calculated *d*-Spacings Found from 2D WAXS Measurements on Samples 1 and 2d

	DEH-PPV[a] (**1**)		DEH-PPV[b] (**1**)		DEH-PPV-P (BA-*stat*-CMS)[a] (**2d**)	
hkl	d_{exp}, Å	d_{calc},[c] Å	d_{exp}, Å	d_{calc},[d] Å	d_{exp}, Å	d_{calc},[e] Å
100	9.49	9.53	9.69	9.82	9.83	9.79
110	6.11	6.28	6.16	6.28		
1–10	5.89	6.05				
	4.84	?				
200	4.78	4.76	4.91	4.91	4.87	4.89
210	4.38	4.19	4.41	4.22	4.42	4.23
2–10/020	4.18	4.05				
120	3.85	3.78	3.89	3.80	3.84	3.84
1–20	3.74	3.68				
300					3.21	3.26

[a] Measurements performed at ambient temperature. [b] Measurement performed at 65 °C. [c] Indexation has been performed to a monoclinic unit cell with $a = 9.53$ Å, $b = 8.1$ Å, and $\gamma = 88°$. [d] Indexation has been performed to a rectangular unit cell with $a = 9.82$ Å and $b = 8.14$ Å. [e] Indexation has been performed to a rectangular unit cell with $a = 9.79$ Å and $b = 8.36$ Å.

found, which, with the exception of the peak at $s = 0.206$ Å^{-1}, can be indexed to a monoclinic unit cell whose corresponding *d*-spacings are summarized in Table 2. The correlation length for the crystalline phase was estimated to 45 nm using Scherrer's equation. By considering the unit cell of the crystalline phase of DEH-PPV to contain only one chain and by taking into account the average molecular length of 6.5 nm, the material

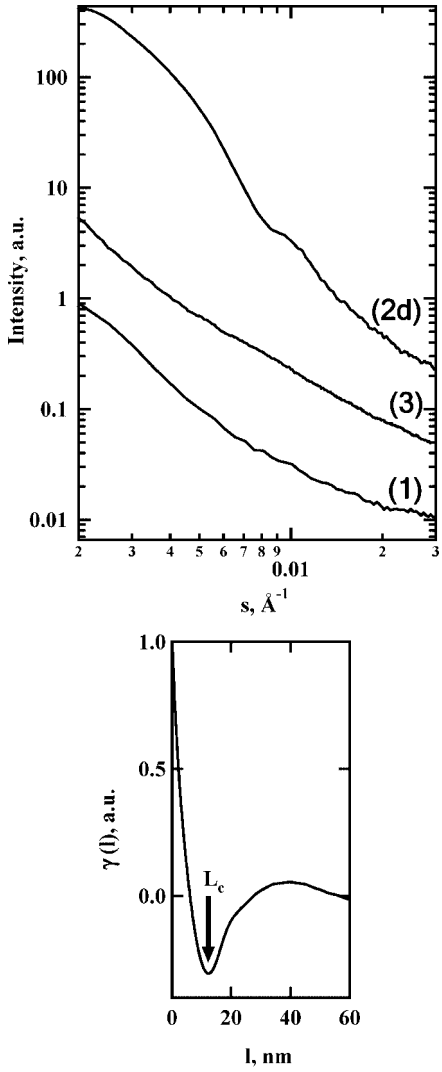

Figure 2. Top: SAXS curves corresponding to DEH-PPV (**1**), DEH-PPV-*b*-poly(BA-*stat*-CMS) (**2d**), and DEH-PPV-*b*-poly(BA-*stat*-C_{60}MS) (**3**) measured at RT. Bottom: one-dimensional SAXS correlation function corresponding to sample **2d**.

density can be estimated to be of the order of 1.09 g/cm^3, which is a reasonable value for polymers. It is noteworthy that no diffraction peak induced by a molecular $\pi-\pi$ stacking (expected around $s = 0.3$ Å^{-1}) has been observed.

The thermal behavior of the sample was studied with temperature-resolved X-ray scattering during sample heating at 10 °C min^{-1}. The WAXS curves measured at 65 and 130 °C are also shown in Figure 1. It can be seen that at 65 °C several diffraction peaks have disappeared, while others are slightly shifted to smaller values of the scattering vector (i.e., to larger distances). We attribute this behavior to a phase transition from a crystalline state to a smectic-like liquid crystalline phase (T_{K-LC}). The temperature evolution of the lattice parameter *a*, given in the inset of Figure 1, reveals indeed a rapid increase with an inflection point at the phase transition temperature, which can be estimated to 55 °C. The tentative assignment of the high-temperature structure to a smectic-like LC phase is based on the presence of multiple sharp reflexes in WAXS. Above ~105 °C, the amplitude reduction of all diffraction peaks indicates further that the material undergoes another transition into a disordered isotropic state (cf. Figure 1).

The SAXS pattern of homopolymer **1** (shown in Figure 2) is featureless even after thermal annealing at 105 °C. This negative result hinders us to determine the structure along the *c*-axis. It also points out that the crystalline order is limited mostly to directions *a* and *b*, leading to the formation of randomly distributed lamellar-shaped crystals with poorly defined thicknesses. This behavior agrees with previous observations done by Olsen et al. on similar materials with various molecular weights.[28] Their results showed in particular that, for molecular weights of 4 kg mol^{-1} or less, polydispersities higher than 1.1 introduce significant interfacial broadening.

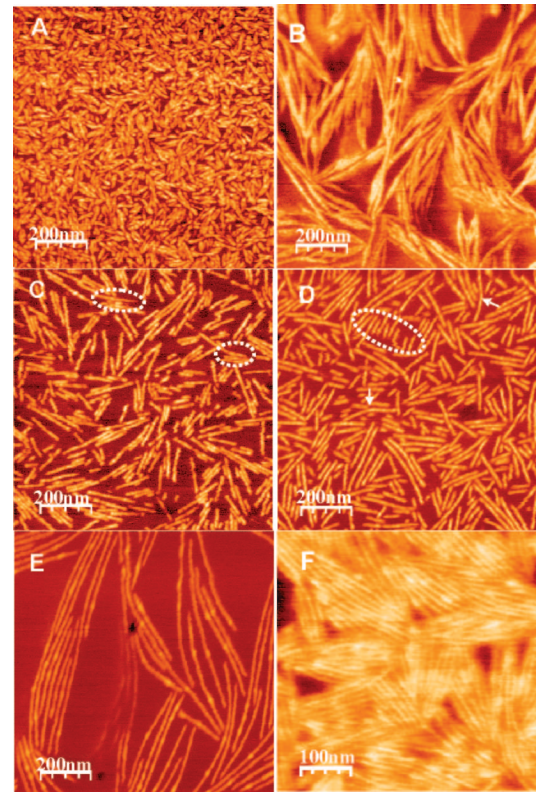

Figure 3. AFM phase images of (A) as-deposited homopolymer **1**, (B) homopolymer **1** after 1 h at 90 °C, (C) as-deposited copolymer **2c**, (D) as-deposited copolymer **2e**, (E) copolymer **2e** after 1 h at 90 °C, and (F) copolymer **2b** after 15 min at 90 °C. The color scale corresponds to phase changes of 10° for (A), 20° for (B), 10° for (C), 5° for (D, E), and 35° for (F).

The tapping-mode AFM phase images obtained on either as-deposited or annealed thin films of homopolymer **1** are reported in Figure 3A,B. In phase images, the image contrast is essentially due to the difference in the tip–sample interaction: soft coil-rich domains appear dark, while brighter regions are associated with harder crystalline domains. For the as-deposited homopolymer **1**, a disordered assembly of elongated objects with an average length of 80 nm and a thickness of the order of 10 nm can be observed. After annealing at 90 °C for 1 h, these structures grow into a disordered mesh of lamellar-type structures of micrometer length and a thickness of roughly 15 ± 5 nm. These observations corroborate the conclusion of the X-ray diffraction experiments that the homopolymer **1** forms lamellar-shaped crystals characterized by a significant lateral disorder and nonuniform thickness.

Fullerene-Free Copolymers. The WAXS diffraction patterns of the fullerene-free copolymers with various coil weight fractions were measured at ambient temperature and are given in Figure 4. Sharp diffraction peaks are visible only for samples with relatively small coils (i.e., **2c** and **2d**) whereas broad amorphous halos are seen for the two other materials (**2f**, **2g**). The *d*-spacings corresponding to the most ordered copolymer **2c** are reported in Table 2. They are close to the values observed

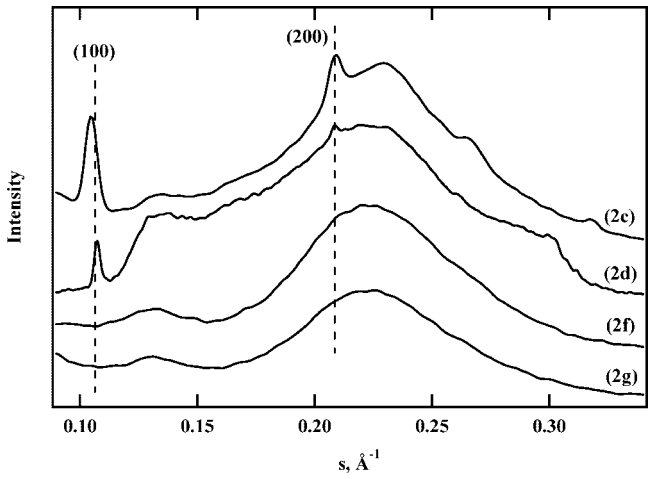

Figure 4. WAXS patterns of DEH-PPV-*b*-poly(BA-*stat*-CMS) copolymers **2c**, **2d**, **2f**, and **2g** measured at RT.

for homopolymer **1** in the LC state and are consistent with the previously reported electron diffraction pattern obtained on copolymer **2b** thin films, where similar diffraction lines were seen.[27] The diffraction pattern disappears upon annealing for all copolymers, with a WAXS clearing temperature, T_{LC-I}, that decreases with increasing coil fraction. For samples **2d**, T_{LC-I} equals 90 °C, which is appreciably lower than that of pure homopolymer **1** (105 °C), while for **2f** and **2g**, the material remains isotropic down to a temperature of at least −50 °C.

The copolymer **2d** SAXS profile (Figure 2) displays a ripple at about $s = 0.08$ Å^{-1}. Such a pattern is related to the form factor of a lamellar-type structure and reveals certain shape uniformity along the normal to the lamellar basal plane. Importantly, the SAXS signal remains visible up to temperatures as high as 166 °C, which is well above the WAXS clearing temperature.

By analyzing the SAXS curve with the classical approach of one-dimensional SAXS correlation (CF) function,[29] $\gamma(l)$, the characteristic size of the structure can be deduced (Figure 2, bottom). This corresponds to the first minimum of the CF located at 12.3 nm. It is noteworthy that the stacking period, which corresponds to the first subsidiary maximum of the CF, is not well-defined, indicating that there is a rather broad distribution of nearest-neighbor distances. Possible reasons for such poor organization of copolymers in the bulk will be discussed in the following.

The X-ray results point out that increasing the coil block length weakens the DEH-PPV structure (as exposed by the reduced T_{LC-I}) and introduces disorder into the DEH-PPV assembly (less WAXS diffraction lines). For the copolymer **2d**, whose coil weight fraction is of medium size, the SAXS results show that microphase separation between both blocks enhances the structural order along the *c*-axis of the liquid-crystalline rod phase and gives rise to lamellae which are visible by SAXS. The SAXS pattern persistence at high temperature further reveals that microphase separation operates even when the rod block is in its disordered state.

The AFM morphology of the copolymer films before annealing differs significantly from that of homopolymer **1** (Figure 3C,D). Stacks of linear fibril-like structures (some of which are indicated by dashed lines) with a remarkably uniform thickness and up to 200 nm in length, surrounded by featureless domains, can be seen. The bright phase contrast points out that these structures are formed by the rod block and are separated by soft, coil-rich domains. This is corroborated by the fact that the separation between fibrils within the stacks tends to be larger for the longer coil block (Figure 3D). The piling up into parallel aligned fibrils, with almost no fibril crossing, suggests that these structures actually may have a significant lateral dimension (along the vertical direction) and form two-dimensional lamellae oriented edge-on rather than one-dimensional fibers. The bending of some fibrils induced by neighboring structures (see arrow in Figure 3D) further substantiates this description. Also, a preliminary transmission electron microscopy investigation, reported in ref 27, supports the 2D nature of these structures. The featureless domains may correspond to lamellae oriented parallel to the substrate, similar to what has been reported on other rod−coil block copolymers.[24,30]

For a coil block weight fraction of 84% (copolymer **2f**), no similar structure could be observed. Interestingly, this result is in agreement with the phase behavior of DEH-PPV-polyisoprene block copolymers for which Olsen et al.[25] found a liquid crystal to isotropic state transition at a coil volume fraction of ∼0.85. Although the differing coil chemical structures do not allow a quantitative comparison between both sets of data, the same qualitative behavior seems to hold for both block copolymers systems.

Annealing at 90 °C leads to a significant growth of the structures in the films of copolymers **2c** and **2e** (Figure 3E). The major features described above (parallel stacking, no crossing, bending) are enhanced and confirm the lamellar nature of the structures. The featureless domains also increase upon annealing and may be attributed to the growth of the horizontal lamellae. A similar behavior can be seen for the copolymer **2b**, with the lowest coil weight fraction (Figure 3F). In this case, however, both the lamellar thickness and the intralamellar distance are reduced (note the reduced image scale), and the proportion of edge-on lamellae has increased.

To investigate in more details the influence of the coil block length on the morphology and to allow a comparison with the results obtained by SAXS, we have performed a quantitative AFM image treatment based on reciprocal space analysis. To this end, one-dimensional power spectral density (PSD) functions were calculated (Figure 5) from the AFM images of as-deposited films, as described earlier.[31,32] Using appropriately modified scaling laws adapted for the case of a 2D space, the SAXS-type one-dimensional correlation and interface distribution functions have been calculated for the PSD functions of the AFM phase images. The results are summarized in Table 3. The most probable lamellar core thickness (L_c) for the fullerene-free copolymer **2e**, determined from the first maximum of the IDF (Figure 5C), was found to be 10.5 ± 0.5 nm, whereas the lamellar stacking period (L_B), corresponding to the first secondary maximum of the CF (Figure 5B) or to the first minimum of the IDF, is 21.6 ± 0.5 nm. The interlamellar distance ($L_a \equiv L_B - L_c$), or lamellar shell thickness, is thus estimated to 11.1 ± 1.0 nm. A similar analysis of the **2c** phase image yields 9.9 ± 0.5 nm for L_c. The corresponding L_B value cannot be evaluated with certainty given the insufficient statistics of the AFM image: it can be seen that the PSD curve of sample **2e** (Figure 5A) exhibits a much more pronounced Bragg peak located at about 0.005 Å^{-1}. Nevertheless, the corresponding IDF indicates that the most probable nearest-neighbor distance is 19.4 ± 0.5 nm. An estimate of L_a for this sample gives then 9.5 ± 0.5 nm. It is however well-known that the reciprocal space treatment can result in confusion of the two distances[33] (i.e., L_c and L_a) due to the Babinet principle. Therefore, the values for the lamellar thickness have been also cross-checked by performing particle analysis of the images as described in ref 33 (the apparent lamellar thickness distributions of Figure 4C,D are shown in the Supporting Information). The values of the most probable lamellar thickness for the copolymers (**2c** and **2e**) are found to be equal to 10.9 ± 0.5 nm. They are almost identical for the two copolymers and close to twice the rod-block length.

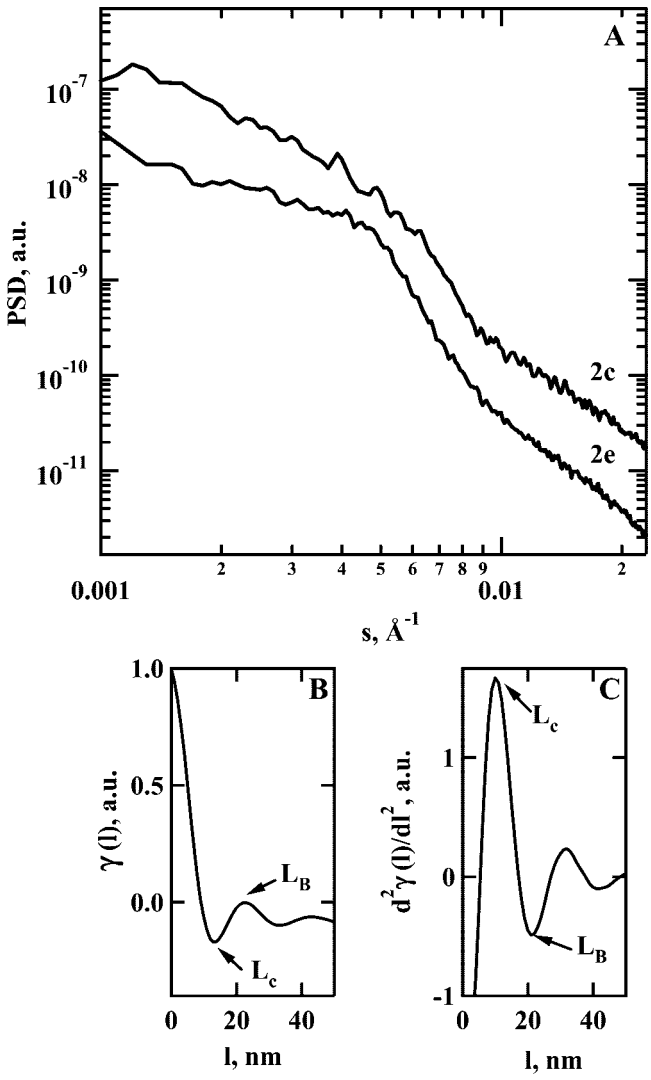

Figure 5. (A) Power spectral density functions calculated from the AFM images in Figure 3C,D. (B, C) One-dimensional SAXS-type correlation and interface distribution functions calculated for the image given in Figure 3D.

Table 3. Lamellar Shell and Core Thickness Obtained by the Correlation Method on Either AFM or SAXS Results for Various Nongrafted Copolymers

copolymer	2b	2c	2d	2e
lamellar core thickness L_c (nm)	6.0 ± 0.5	9.9 ± 0.5	13.0 ± 0.2	10.5 ± 0.5
lamellar shell thickness L_a (nm)	6.2 ± 0.7	9.5 ± 0.7		10.1 ± 0.7
method	AFM	AFM	SAXS	AFM

In the case of the copolymer with the lowest rod−coil weight ratio (**2b**) however, a similar analysis of the AFM phase image (Figure 3F) leads to a lamellar core thickness of only 6.2 nm, slightly lower than the rod length (estimated to 7.8 nm for copolymer **2b**). These results suggest that lamellae may be formed either of rod-block monolayers or bilayers, depending on the copolymer molecular structure. The conditions needed to achieve either of these structures appear to depend critically on the rod−coil block ratio and on the rod-block polydispersity index, which was lower in the case of copolymer **2b**. However our investigations are not sufficient to allow us to identify the conditions (in terms of molecular structure), which lead to either single- or double-layer lamellar phase or to an amorphous structure. This would require a more systematic investigation, which is beyond the scope of the present work.

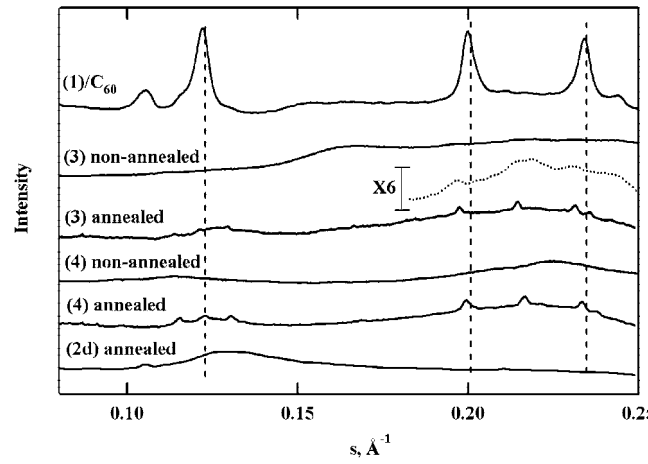

Figure 6. WAXS curves of a blend of DEH-PPV (**1**) and C_{60}; fullerene-grafted copolymer **3** before annealing with enlarged fragment (dashed line); fullerene-grafted copolymer **3** after 4 h annealing at 90 °C; poly(butyl acrylate-*stat*-C_{60}MS) (**4**) before annealing; poly(butyl acrylate-*stat*-C_{60}MS) (**4**) after 4 h annealing at 90 °C; and DEH-PPV-*b* poly(BA-*stat*-CMS) (**2d**) after 4 h annealing at 90 °C.

Fullerene-Grafted Copolymers. The WAXS patterns of the fullerene-grafted copolymer **3**, before and after annealing, are shown in Figure 6. Also shown are the patterns obtained on an as-deposited blend of homopolymer **1** with an amount of free C_{60} molecules equivalent to the fullerene content of **3** and those of the poly(butyl acrylate-*b*-C_{60}MS) (PBA-C_{60}) copolymer **4**, before and after annealing. The results obtained on **3** show several broad diffraction peaks as well as a number of smaller relatively narrow peaks, whose amplitude increases upon annealing. These peaks differ significantly from those characteristic of the copolymer structure which appear in the diffractogram of the annealed sample **2d** (also shown in Figure 6 for comparison). On the other hand, the peak positions are close to those found either on copolymer **4** or on the blend of homopolymer **1** and free C_{60}. The three major peaks observed in the blend coincide with those expected for pure C_{60} crystals according to ref 34 except for the peak at 0.106 $Å^{-1}$ which corresponds to the homopolymer crystalline structure. The broadening of the peak at 0.122 $Å^{-1}$ can be induced by the broad diffraction halos observed for the homopolymer **1** (Figure 2). The peaks of **3** and **4** can be indexed to a monoclinic lattice differing slightly from that of pure C_{60} crystals. The corresponding *d*-spacings are given in the Supporting Information. Interestingly, the corresponding lattice parameters are very close to those found for the crystalline lattice of the fullerene derivative [6,6]-phenyl-C[61]-butyric acid methyl ester (PCBM) reported elsewhere.[35]

The good agreement between the diffraction pattern of the blend and that of pure C_{60}, establishes that fullerene nanocrystals have been formed in the blend. On the other hand, the successful indexation of the diffraction peaks of **3** and **4** to a monoclinic structure similar to that of PCBM strongly suggests that distorted C_{60} nanocrystals are formed in these materials even though the fullerenes are covalently bonded to a polymer backbone. The observed trend toward larger lattice parameters, illustrated by a shift to smaller angles of the diffraction peaks when comparing free C_{60} with polymer **4** and with copolymer **3** (see Supporting Information), reflects the influence of the C_{60}−polymer covalent bond on the fullerene crystallization. The indexation of the C_{60} related diffraction peaks reveals a distortion of the C_{60} cubic phase and the formation of a less dense crystalline structure. This behavior is most pronounced in the case of the copolymer **3.** The average size of C_{60} crystallites in **3** and **4**, deduced from the peak shape, is ∼90 ± 30 nm.

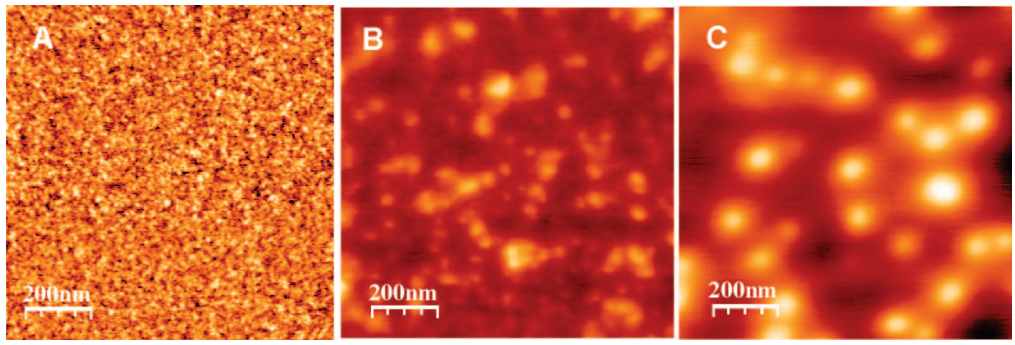

Figure 7. (A) AFM phase image of as-deposited fullerene-grafted copolymer **3** (color scale: 25°). (B) AFM topography of **3** after 1 h at 90 °C (color scale: 20 nm). (C) Drop-casted polymer **4** (color scale: 20 nm).

The absence of the rod-block-related diffraction peaks (observed in the material before fullerene grafting, i.e., in copolymer **2d**) in the spectra of **3** points out that no ordered rod phase could form. This is further corroborated by the fact that the SAXS pattern of **3**, shown in Figure 2, is featureless. Both WAXS and SAXS data therefore point out that the presence of C_{60} moieties impedes the self-assembling process for the copolymer. The situation is different for the blend with C_{60}, for which the crystallization of fullerene does not interfere with the rod-block crystallization in the blend, as suggested by the presence of the DEH-PPV diffraction peak. On the other hand, grafting the fullerene onto the polymer does not hinder the formation of fullerene nanocrystals. Only the crystal growth is slowed down by the presence of the rod and coil blocks since no structures are observed in **3** and **4** prior to annealing. Note that the annealing temperature was below the highest temperature used during the fullerene grafting procedure (120 °C). Therefore, thermally induced dissociation of the polymer-fullerene bond and subsequent crystallization of released C_{60} molecules can be excluded. Inclusion of some residual free fullerene molecules into the observed crystals is possible but should be much lower than 10% of the total amount of C_{60} (i.e., nonreacted C_{60} before the purification step, estimated from the residual azide groups seen by FTIR).

The AFM morphology of the fullerene-grafted copolymer **3**, shown in Figure 7, differs significantly from that of the homopolymer and the fullerene-free copolymers. Before annealing, no lamellar structures can be identified on the phase image (Figure 7A). The nevertheless significant phase contrast may be due to either local variations in composition or roughness induced phase changes (the rms film roughness deduced from topographical images was estimated to 0.4 nm). After 1 h annealing at 90 °C, the formation of nanoparticles, best seen in the topographical image (Figure 7B), occurs. Interestingly, similar particles are present in an as-desposited film of the fullerene-grafted polymer **4** (Figure 7C). These results agree with the X-ray diffraction data. The absence of lamellar-type structures in the AFM image of copolymer **3** are consistent with the featureless SAXS data. Furthermore, the formation of nanoparticles in thin films of both fullerene-grafted materials (**3** and **4**) can be related to the WAXS diffraction peaks seen in the corresponding bulk materials. A reasonable matching is also found between the average size of the particles estimated from WAXS and AFM measurements. Both results suggest that grafted C_{60} molecules strongly tend to form nanocrystals, thereby hindering significantly the copolymer self-assembling process, which otherwise would lead to a lamellar-type morphology.

Optical Properties. An additional insight into the intermolecular interactions resulting from the block copolymer self-assembling process can be gained from the optical thin film properties. Figure 8 displays the UV absorption spectra of the homopolymer and copolymers. The absorption spectra of the

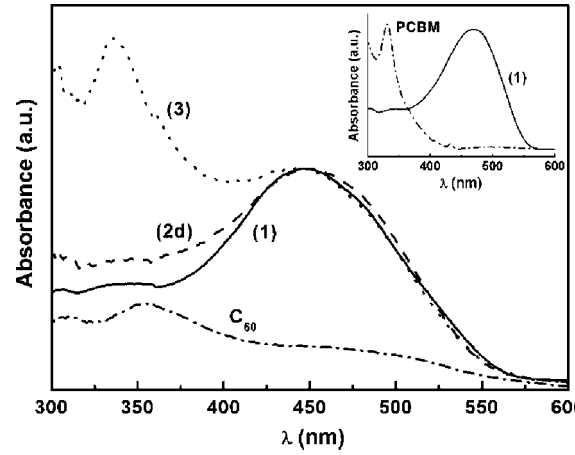

Figure 8. Absorption spectra of **1**, **2d**, and pristine C_{60} thin films. The inset shows the absorption spectra of a soluble C_{60} derivative (PCBM) and of the homopolymer **1** in chloroform.

homopolymer in solution and that of a soluble C_{60} derivative ([6,6]-phenyl-C[61]-butyric acid methyl ester, or PCBM) in either solution or solid state are shown for comparison. The absorption band around 450 nm, observed in all copolymer films, is due to DEH-PPV $\pi-\pi^*$ transitions. A 20 nm blue shift of the absorption maximum is seen when going from solution to the film. This behavior points out that for both homopolymer and copolymer films $\pi-\pi$ stacking interactions, which should red-shift the $\pi-\pi^*$ absorption band, are insignificant and is consistent with the absence of a characteristic $\pi-\pi$ stacking signature in the homopolymer WAXS profile. The additional disorder in the LC state (fullerene-free copolymer) or in the amorphous state (fullerene-grafted copolymer **3**) does not modify the rod−block interactions significantly enough to affect its optical properties. On the other hand, the absorption band induced by the fullerene HOMO–LUMO gap is significantly altered when going from solution to thin films. The 6 nm red shift in the case of **3** is due to C_{60} aggregation and corroborates the X-ray diffraction data, which revealed the presence of C_{60} nanocrystals. The red shift is less pronounced than for pristine C_{60} films (about 25 nm) and can be linked to the less dense packing of grafted C_{60} (as revealed by the X-ray diffraction data).

The thin film photoluminescence (PL) spectra of homopolymer **1** and of copolymers **2d** and **3** have also been measured (the PL results can be seen in the Supporting Information) and revealed a significant PL quenching in the fullerene-grafted material. This suggests that efficient exciton dissociation takes place at the C_{60}/DEH-PPV interface, although the existence of nonradiative recombination mechanism cannot be excluded. It is worth noticing that a relatively small amount of grafted C_{60} (2.5 fullerene moieties per molecule, which corresponds to ~21

wt % ratio) is sufficient for an efficient luminescence quenching. This result puts forward a large donor–acceptor interface, which in turn is related to the nanometric size of the grafted fullerene nanocrystals.

General Discussion. The results obtained on both bulk materials and thin films allow a better understanding of the self-assembling process of the fullerene-grafted rod−coil copolymers. Three major driving forces for the self-assembly, which may either be in competition or act in conjunction, can be identified: (i) the π-system-mediated rod−rod interactions, which are responsible for the formation of liquid crystalline and crystalline lamellae, (ii) the microphase separation between the rigid conjugated block and the flexible coil block, which for low enough coil weight fractions can trigger the formation of a lamellar morphology with intralamellar order, and (iii) aggregation of grafted C_{60} molecules which leads to the formation of fullerene nanocrystals.

Their relative strengths will determine the thin film morphology and make it more or less appropriate for the photovoltaic applications. Ideally, rod crystallization and microphase separation should both lead to the formation of well-defined nanodomains of lamellar shape and restrict the fullerene crystallization within the coil-rich domains, giving rise to interpenetrated donor–acceptor nanoscale networks. The molecular ordering within the domains will determine the electronic quality of the resulting morphology, as efficient charge transport generally relies on strong intermolecular $\pi-\pi$ interactions.

In the case of the copolymers investigated in this work, the rod-block interactions turn out to be the weakest driving force. The higher SAXS clearing temperature, with respect to the WAXS data, indicates indeed that, on cooling, the microphase separation occurs prior to the formation of the smectic LC phase. The lower LC−I transition temperature of the fullerene-free copolymer, with respect to the conjugated homopolymer, and the absence of a crystalline phase at room temperature also point out that the coil block significantly destabilizes the rod−rod interactions within the lamellae. The weak rod−rod interactions are related to the large intermolecular distances of the DEH-PPV in its crystalline phase, which, according to the WAXS data, are estimated to be of the order of the lattice parameter (8.1 Å) and to the absence of $\pi-\pi$ stacking interactions. For nongrafted copolymers with sufficiently low coil weight fractions, this process leads to a smectic-like liquid-crystalline state rather than to a crystalline state.

The missing evidence for the formation of a well-ordered lamellar stacking in the bulk, which should have been revealed by a series of sharp Bragg peaks in SAXS curves, as was the case for the rod−coil copolymers studied in ref 24 is puzzling. Indeed, lamellar structures with uniform thickness are clearly visible in the AFM images, and in some cases, such as that of **2e**, the lamellar stacking in 2D is clearly observed. A possible reason for poor lamellar ordering in the bulk could be due to their small lateral dimensions, which in the thin film configuration is below the film thickness (between 80 and 100 nm). Furthermore, in a recent paper,[36] it was shown that copolymers with rather long coils form morphologies different from lamellar. Therefore, we can speculate that the lamellar stacking, which is sometimes clearly developed in the edge-on oriented lamellae in thin films, can display different order in 3D.

The absence of any lamellar signature in the case of the fullerene-grafted copolymer shows that the fullerene aggregation dominates the molecular assembling of our material. Small C_{60} crystals are able to form despite the fact that the fullerene moieties are covalently linked to the coil block. Given the high stability of C_{60} crystals (as revealed by the WAXS pattern at high temperature), we hypothesize that the C_{60} aggregation starts while the rod segments are still in their isotropic state. The formation of these crystals is likely to impede the copolymer microphase separation during cooling or solvent evaporation. In other words, even if the thermodynamic equilibrium configuration of the fullerene-grafted molecules corresponds eventually to a lamellar morphology, the fullerene aggregation introduces a kinetic barrier that impedes the formation of rod and coil nanodomains.

The resulting thin film morphology is unfortunately still far from the target nanostructure and leads to photovoltaic devices with poor performances.[37] Although the significant photoluminescence quenching suggests the presence of a large donor–acceptor interface, insufficient charge transport across the disordered copolymer layer is presumably the major limiting factor. Different strategies can be considered to circumvent these limitations. The rod−rod interactions could be enhanced by using conjugated segments which allow better $\pi-\pi$ stacking interactions. Polythiophene derivatives, which are well-known to form highly ordered structures, are possible candidates.[38] Increasing the rod-block length may also lead to a similar improvement but is limited by chemical synthesis. Stronger rod−rod interactions may eventually lead to crystalline lamellae and thereby improve the charge carrier mobility. Another possibility would be to use different acceptor groups such as sterically hindered fullerene derivatives or perylene moieties with reduced tendency to agglomerate. Blending the copolymers with homopolymers may be an additional option. Sary et al. indeed observed recently that the presence of even minor fractions of rod homopolymers in a homopolymer/rod−coil copolymer blend strongly enhances the formation of lamellar structures.[39] A similar approach with fullerene-grafted copolymers may be enough to counterbalance the strong driving force of C_{60} crystallization. At last, replacing the covalent fullerene−coil bond by weaker supramolecular interaction mechanisms may be another way to attenuate the interference between fullerene crystallization and copolymer self-assembling.[40]

Conclusion

A series of novel fullerene-grafted rod−coil block copolymers, designed for being used as active layer in photovoltaic devices, were synthesized by controlled/"living" radical polymerization. The highly soluble poly[(2,5-di(2′-ethyl)hexyloxy)-1,4-phenylenevinylene] was used as a conjugated rod block while poly(butyl acrylate-*stat*-chloromethylstyrene) copolymer, with various chloromethylstyrene (CMS) content, was used as coil block. The fullerene grafting reaction by CMS azidation was monitored with infrared absorption spectroscopy and ^{1}H NMR. The molecular self-assembling processes, in bulk materials and in thin films, were studied by X-ray diffraction, atomic force microscopy, UV–vis absorption, and photoluminescence measurements. The molecular structure−morphology relationship was investigated by analyzing the behavior of rod-block homopolymers and rod−coil block copolymers, before and after fullerene grafting.

We found that the rod block alone crystallizes at room temperature into lamellar phase with a monoclinic unit cell. The temperature-dependent X-ray diffraction measurements further revealed a crystalline to liquid-crystalline smectic phase transition. For the fullerene-free copolymer with a sufficiently low rod−coil weight fraction, the coil block destabilizes considerably the rod−rod interactions and leads to a lamellar phase with the rod block being in a liquid-crystalline state at room temperature. On the other hand, microphase separation enhances the interlamellar ordering. The lamellar geometrical parameters were deduced from both AFM and X-ray results by using the one-dimensional correlation function approach. The results show that either monolayer or double-layer lamellae were formed, depending on the copolymer molecular structure. Adding the fullerene

moieties considerably affects the polymer self-assembly through the growth of fullerene nanocrystals. The latter hinder the formation of the lamellar phase by pinning the coils. Although a strong photoluminescence quenching suggests the presence of a large donor–acceptor interface, the resulting thin film nanostructure remains inappropriate for the target bulk heterojunction photovoltaic device. The identification of the major driving forces that control the molecular self-assembling process nevertheless allowed us to suggest different alternative strategies that can be used as guidelines for the design of new photovoltaic polymer self-assembling materials.

Experimental Section

Chemicals and Methods. Tetrahydrofuran (THF) and toluene were distilled from Na/benzophenone, diethyl ether from $LiAlH_4$, and dichloromethane from CaH_2; dimethylformamide (DMF) and triethylamine were dried on activated molecular sieves (4 Å). Column chromatography was performed using silica gel (Merck Geduran Si 60 (40–63 μm)). All other chemicals and solvents were used as received, and all reactions were performed under dry Ar atmosphere, unless noted otherwise. DEH-PPV-TIPNO macroinitiator **1** bearing a 2,2,5-trimethyl-4-phenyl-3-azahexane-3-oxyl nitroxide (TIPNO) alkoxyamine has been synthesized according to a procedure reported elsewhere.[41,42]

Synthesis of DEH-PPV-*b*-P(BA-*stat*-CMS) Block Copolymer (2). Macroinitiator **1** was dissolved in specific amounts of BA and CMS, and 5 mol % of free TIPNO was added. The mixture was degassed by three freeze–pump–thaw cycles and placed under an Ar atmosphere or sealed under vacuum. The reaction vessel was immersed in a preheated oil bath at 125 °C. Polymerization was stopped at different times, and the mixture was precipitated twice in cold methanol (−20 °C). Residual homopolymers have been removed via column chromatography, using cyclohexane/dichloromethane (CH_2Cl_2) 1:1 as an eluent. The copolymer has been collected by flushing the column with ethyl acetate. Representative ^{1}H NMR ($CDCl_3$) spectra of DEH-PPV-*b*-P(BA-*stat*-CMS) are: δ (ppm) = 7.6–7.0 (m arom C*H* [DEH-PPV and CMS]), 4.5 (br s, CH_2*Cl* [CMS]), 4.2–3.7 (m, OCH_2 [DEH-PPV and *n*-BA]), 2.5–0.7 (m, aliph C*H* and CH_2 [DEH-PPV], main chain C*H* and CH_2 [P(BA-*stat*-CMS)] and aliph CH_3 [DEH-PPV and *n*-BA]).

Synthesis of DEH-PPV-*b*-P(BA-*stat*-C_{60}MS) (3). The DEH-PPV-*b*-P(BA-*stat*-CMS) copolymer **2d** (see Table 1) was used for the C_{60} grafting reaction, shown in Scheme 2, according to a previously described method.[42] The copolymer was dissolved in DMF (20 mg mL^{-1}), and 20 equiv of NaN_3 was added. After stirring the reaction mixture for 24 h at 50 °C, water and brine were added, and the water phase was extracted with CH_2Cl_2 three times. The combined organic layers were washed with water three times, dried on $MgSO_4$, filtered, and evaporated under reduced pressure. In ^{1}H NMR ($CDCl_3$), the CH_2*Cl* peak shifted from δ (ppm) = 4.55 to 4.31.

The azidated copolymer was dissolved in dichlorobenzene (20 mg mL^{-1}) in a dark reaction vessel, and 1 equiv of C_{60} per N_3MS was added. The solution was degassed by bubbling Ar through. The reaction mixture was stirred in the dark at 60 °C for 24 h and an additional 1 h at 120 °C. The solution was used without further purification and stored under an Ar atmosphere in the dark. The reaction of N_3 with C_{60} has been monitored by ^{1}H NMR and by Fourier-transform infrared spectroscopy (FTIR).

Synthesis of P(BA-*stat*-C_{60}MS) (4). The 2,2,5-trimethyl-3-(1-phenylethoxy)-4-phenyl-3-azahexane alkoxyamine[43] was dissolved in specific amounts of BA and CMS (molar feed ratio monomers/alkoxyamine: 48.5), and 5 mol % of free TIPNO was added. The BA/CMS initial ratio in the reaction mixture was 32/1. The mixture was degassed by three freeze–pump–thaw cycles and sealed under vacuum. The reaction vessel was immersed in a preheated oil bath at 125 °C. Polymerization was stopped after 48 h, and the mixture was precipitated twice in cold methanol (−20 °C). The molecular weight of the copolymer obtained was 3.9 kg mol^{-1}, its polydispersity was 1.2 (estimated by GPC), and the BA/CMS composition was 13/1. This copolymer has been azidated and C_{60} grafted following the procedure described before.

Characterization. ^{1}H NMR spectra were recorded on a Bruker 300 UltrashieldTM 300 MHz NMR spectrometer, with an internal lock on the 2H signal of the solvent ($CDCl_3$). Size exclusion chromatography (SEC) measurements were performed in THF or chloroform (HPLC grade) with two PL-gel 5 μ mixed-C, a 5 μ 100 Å, and a 5 μ Guard column in a Shimadzu LC-10AD liquid chromatograph equipped with a Shimadzu RID-10A refractive index detector and a Shimadzu SPP-M10A diode array (UV) detector. Molecular weights and polydispersity indexes were calculated from a calibration with polystyrene standards. The FTIR spectra were recorded in transmission mode using a Bruker Equinox 55 Fourier spectrophotometer.

X-ray Diffraction. The thermal and structural properties of bulk materials have been investigated by X-ray scattering. Wide-angle X-ray scattering (WAXS) and small-angle X-ray scattering (SAXS) experiments were carried out on the BM26B beamline at the European Synchrotron Radiation Facility (E.S.R.F.) in Grenoble, France. The measurements were performed in transmission mode on oriented samples (fibers with diameter of 0.7 mm) prepared by extrusion at 80 °C using a homemade mini-extruder. The wavelength of 1.24 Å was used. Dynamic measurements were carried out during heating in a Linkam heating stage at 10 °C/min using an acquisition time of 30 s.

Thin Films Preparation. Thin films were prepared by spin-coating 1 wt % chloroform or 1,2-dichlorobenzene solutions onto freshly cleaved mica substrates. The chloroform is a good solvent for both DEH-PPV and poly(butyl acrylate). The fullerene grafting took place in 1,2-dichlorobenzene. To avoid polymer aggregation, the fullerene-grafted copolymer **3** was kept in solution until its deposition by spin-coating. Thin film deposition was done under a nitrogen atmosphere using a rotational speed of 2000 rpm for 180 s. Prior to characterization, the films were stored under primary vacuum overnight in order to eliminate any residual solvent. The resulting layer thickness was between 60 and 80 nm. Thin film annealing at 90 °C was done in a nitrogen atmosphere.

Atomic Force Microscopy. The film surface morphology was investigated by atomic force microscopy (AFM) in tapping mode using topography and phase imaging. Silicon microcantilevers with a spring constant of 21–98 N/m and a resonance frequency of 146–236 kHz were used.

The sample thermal treatments were done under a nitrogen atmosphere in order to avoid oxidative polymer degradation.

Absorption and Fluorescence. Thin film and solution absorption spectra were acquired by a Shimadzu UV-2101 spectrophotometer. The photoluminescence (PL) spectra were measured by exciting the samples with a monochromatic light source at λ = 355 nm from a ND:YW04 laser of 100 mW. For optical characterizations, the films were prepared by drop-casting 1 wt % 1,2-dichlorobenzene (DCB) solutions onto NaCl substrates.

Acknowledgment. The authors thank the French National Agency for Research (ANR), the Region Alsace, the SOPREMA Co., and the European Community for financial support through the NANORGYSOL, MONACOP, and FAMOUS programs. They gratefully acknowledge Jérémy Bartinger for the FTIR and PL measurements and Patrick Lévêque as well as Nicolas Leclerc for stimulating discussions and their critical reading of the manuscript. D.A.I. acknowledges financial support from the ATIP project of the CNRS (France) and the European Community's "Marie-Curie Actions" under Contract MRTN-CT-2004-504052 [POLYFILM]. We acknowledge the European Synchrotron Facility and NWO for provision of beam time and thank W. Bras, K. Kvashnina, and N. Vilayphiou for technical assistance.

Supporting Information Available: FTIR spectra of materials **1**, **2d** before and after azidation, and **3**; lamellar thickness distribution from particle analysis in **2a** and **2d** thin films; experimental and calculated *d*-spacings for materials **3** and **4**;

photoluminescence spectra of **1**, **2d**, and **3** thin films. This material is available free of charge via the Internet at http://pubs.acs.org.

References and Notes

(1) Heeger, A. J. *J. Phys. Chem. B* **2001**, *105*, 8475–8491.
(2) Saraciftci, N. S.; Smilowitz, L.; Heeger, A. J.; Wudl, F. *Science* **1992**, *258*, 1474–1476.
(3) Granström, M.; Petritsch, K.; Arias, A. C.; Lux, A.; Andersson, M. R.; Friend, R. H. *Nature (London)* **1998**, *395*, 257–260.
(4) Coakley, K. M.; McGehee, M. D. *Chem. Mater.* **2004**, *16*, 4533–4542.
(5) Brabec, C. J. *Sol. Energy Mater. Sol. Cells* **2004**, *83*, 273–292.
(6) Martens, T.; D'Haen, J.; Munters, T.; Beelen, Z.; Goris, L.; Manca, J.; D'Olieslaeger, M.; Vanderzande, D.; de Schepper, L.; Andriessen, R. *Synth. Met.* **2003**, *138*, 243–247.
(7) Hoppe, H.; Niggemann, M.; Winder, C.; Kraut, J.; Hiesgen, R.; Hinsch, A.; Meissner, D.; Saraciftci, N. S. *Adv. Funct. Mater.* **2004**, *14*, 1005–1011.
(8) Zhang, F. L.; Johansson, M.; Andersson, M. R.; Hummelen, J. C.; Inganäs, O. *Synth. Met.* **2003**, *137*, 1401.
(9) Reyes-Reyes, M.; Kim, K.; Dewald, J.; Lopez-Sandoval, R.; Avadhanula, A.; Curran, S.; Carroll, D. L. *Org. Lett.* **2005**, *7*, 5749–5752.
(10) Kim, J. Y.; Lee, K.; Coates, N. E.; Moses, D.; Nguyen, T.-Q.; Dante, M.; Heeger, A. J. *Science* **2007**, *317*, 222–225.
(11) Lemaur, V.; Steel, M.; Beljonne, D.; Bredas, J. L.; Cornil, J. *J. Am. Chem. Soc.* **2005**, *127*, 6077–6086.
(12) Hoppe, H.; Saraciftci, N. S. *J. Mater. Chem.* **2005**, *16*, 45–61.
(13) Stalmach, U.; de Boer, B.; Videlot, C.; van Hutten, P. F.; Hadziioannou, G. *J. Am. Chem. Soc.* **2000**, *122*, 5464–5472.
(14) de Boer, B.; Stalmach, U.; van Hutten, P. F.; Meltzer, C.; Krasnikov, V. V.; Hadziioannou, G. *Polymer* **2001**, *42*, 9097–9109.
(15) Sun, S.-S. *Sol. Energy Mater. Sol. Cells* **2003**, *79*, 257–264.
(16) Lindner, S. M.; Hüttner, S.; Chiche, A.; Thelakkat, M.; Krausch, G. *Angew. Chem., Int. Ed.* **2006**, *45*, 3364–3368.
(17) Krebs, F. C.; Hagemann, O.; Jørgensen, M. *Sol. Energy Mater. Sol. Cells* **2004**, *83*, 211–228.
(18) Sun, S. S.; Zhang, C.; Ledbetter, A.; Choi, S.; Seo, K.; Drees, M.; Saricifici, N. S. *Appl. Phys. Lett.* **2007**, *90*, 043117–043119.
(19) Lindner, S. M.; Thelakkat, M. *Macromolecules* **2004**, *37*, 8832–8835.
(20) Segalman, R. A.; Brochon, C.; Hadziioannou, G. *Organic Photovoltaics: Mechanisms, Materials, and Devices*; Sun, S.-S., Sariciftci, N. S., Eds.; Taylor & Francis: London, 2005; pp 403−420.
(21) Liang, Y.; Wang, H.; Yuan, S.; Lee, Y.; Gan, L.; Yu, L. *J. Mater. Chem.* **2007**, *17*, 2183–2194.
(22) Bates, F. S.; Frederickson, G. H. *Phys. Today* **1999**, *52*, 32.
(23) Matsen, M. W.; Barrett, C. *J. Chem. Phys.* **1998**, *109*, 4108–4118.
(24) Olsen, B. D.; Segalman, R. *Macromolecules* **2005**, *38*, 10127–10137.
(25) Olsen, B. D.; Segalman, R. *Macromolecules* **2006**, *39*, 7078–7083.
(26) Olsen, B. D.; Segalman, R. A. *Macromolecules* **2007**, *40*, 6922–6929.
(27) Heiser, T.; Adamopoulos, G.; Brinkmann, M.; Giovanella, U.; Ould-Saad, S.; Brochon, C.; van de Wetering, K.; Hadziioannou, G. *Thin Solid Films* **2006**, *511–512*, 219–223.
(28) Olsen, B. D.; Jang, S.-Y.; Lüning, J. M.; Segalman, R. *Macromolecules* **2006**, *39*, 4469–4479.
(29) (a) Ruland, W. *Colloid Polym. Sci.* **1977**, *255*, 417. (b) Balta-Calleja, F. J.; Vonk, C. G. *X-ray Scattering of Synthetic Polymers*; Elsevier: Amsterdam, 1989.
(30) Olsen, B. D.; Li, X.; Wang, J.; Segalman, R. A. *Macromolecules* **2007**, *40*, 3287–3295.
(31) Basire, C.; Ivanov, D. A. *Phys. Rev. Lett.* **2000**, *85*, 5587.
(32) Ivanov, D. A.; Magonov, S. In *Polymer Crystallization: Observations, Concepts and Interpretations*; Sommer, J. U., Reiter, G., Eds.; Springer-Verlag: Berlin, 2003; pp 98–129.
(33) Ivanov, D. V.; Legras, R.; Jonas, A. M. *Macromolecules* **1999**, *32*, 1582–1592.
(34) W. I. F., David.; R. M., Ibberson.; J. C., Matthewman.; K., Prassides.; T. J. S., Dennis.; J. P., Hare.; H. W., Kroto.; R., Taylor.; Walton, D. R. M. *Nature (London)* **1991**, *353*, 147–149.
(35) Rispens, M. T.; Meetsma, A.; Rittberger, R.; Brabec, C. J.; Sariciftci, N. S.; Hummelen, J. C. *Chem. Commun.* **2003**, 2116–2118.
(36) Olsen, B. D.; Segalman, R. A. *Macromolecules* **2007**, *40*, 6922–6929.
(37) For this experiment, a standard device structure, using an indium−tin oxide and PEDOT:PSS film on a glass substrate as anode and a thin aluminium layer as cathode, was fabricated and characterized. The measured short-circuit photocurrent under a AM1.5 solar simulator was 5 μA/cm^2 while the open-circuit voltage was close to 0.2 V. The energy conversion efficiency of reference devices, fabricated with the same procedure and in the same environment, using blends of soluble polythiophene (P3HT) and fullerene derivatives (PCBM) reached values as high as 4.5%.
(38) Richard, F.; Brochon, C.; Eckhardt, D.; Ngov, C.; Leclerc, N.; Barrau, S.; Bechara, R.; Lévêque, P.; Heiser, T.; Hadziioannou, G. EPF European Polymer Congress, Portoroz, Slovenia, Extended abstract, OC5.3.28, **2007**.
(39) Sary, N.; Mezzenga, R.; Brochon, C.; Hadziioannou, G.; Ruokolainen, J. *Macromolecules* **2007**, *40*, 3277–3286.
(40) Sary, N.; Rubatat, L.; Brochon, C.; Hadziioannou, G.; Ruokolainen, J.; Mezzenga, R. *Macromolecules* **2007**, *40*, 6990–6997.
(41) Stalmach, U.; de Boer, B.; Post, A. D.; van Hutten, P. F.; Hadziioannou, G. *Angew. Chem., Int. Ed.* **2001**, *40*, 428–430.
(42) van der Veen, M. H.; de Boer, B.; Stalmach, U.; van de Wetering, K. I.; Hadziioannou, G. *Macromolecules* **2004**, *37*, 3673–3684.
(43) Benoit, D.; Chaplinksi, V.; Braslau, R.; Hawker, C. J. *J. Am. Chem. Soc.* **1999**, *121*, 3904–3020.

MA7022099